

Article

icMRCI+Q Study of the Spectroscopic Properties of the 14 Λ -S and 49 Ω States of the SiN^- Anion in the Gas Phase

Wei Xing^{1,2}, Jinfeng Sun^{1,3,*}, Deheng Shi³ and Zunlue Zhu³

¹ School of Materials Science and Engineering, Henan University of Science and Technology, Luoyang 471023, China; wei19820403@163.com

² College of Physics and Electronic Engineering, Xinyang Normal University, Xinyang 464000, China

³ College of Physics and Material Science, Henan Normal University, Xinxiang 453007, China; scattering@sina.com.cn (D.S.); zl-zhu@htu.edu.cn (Z.Z.)

* Correspondence: jfsun@haust.edu.cn

Received: 26 November 2017; Accepted: 16 January 2018; Published: 20 January 2018

Abstract: This paper calculates the potential energy curves of the 14 Λ -S and 49 Ω states, which come from the first three dissociation channels of the SiN^- anion. These calculations are conducted using the valence internally contracted multireference configuration interaction and the Davidson correction approach. Core-valence correlation and scalar relativistic corrections are taken into account. The potential energies are extrapolated to the complete basis set limit. The spin-orbit coupling is computed using the state interaction approach with the Breit–Pauli Hamiltonian. We found that the $X^1\Sigma^+$ ($v'' = 0-23$) and $a^3\Sigma^+$ ($v' = 0-2$) states of SiN^- are stable at the computed adiabatic electron affinity value of $23,262.27 \text{ cm}^{-1}$ for SiN . Based on the calculated potential energy curves, the spectroscopic parameters and vibrational levels were determined for all stable and metastable Λ -S and Ω states. The computed adiabatic electron affinity of SiN and the spectroscopic constants of SiN^- ($X^1\Sigma^+$) are all in agreement with the available experimental data. The $d^3\Sigma^+$, $2^5\Sigma^+$, $1^5\Delta$, and $1^5\Sigma^-$ quasi-bound states caused by avoided crossings were found. Calculations of the transition dipole moment of $a^3\Sigma^+_1$ to $X^1\Sigma^+_{0+}$ are shown. Franck-Condon factors, Einstein coefficients, and radiative lifetimes of the transition from the $a^3\Sigma^+_1$ ($v' = 0-2$) to the $X^1\Sigma^+_{0+}$ state are evaluated.

Keywords: spectroscopic parameter; electron affinity; spin-orbit coupling effect; Franck-Condon factor; radiative lifetime

1. Introduction

SiN^- is analogous with the known interstellar CN^- anion [1]. Several silicon-containing nitrogen chains (SiN , SiCN , and SiNC) have been detected in the interstellar medium [2–4]. Consequently, SiN^- is a tantalizing potential interstellar anion candidate [5]. Furthermore, the SiN^- anion is a compound of considerable importance in gas-phase ion chemistry [6], laser-induced plasmas [7], semiconductor chemistry [8], and microelectronics [9]. However, very few experiments [10] and computations [11–16] have been conducted for its spectroscopic properties. Based on the aforementioned facts, we systematically investigated the spectroscopic properties of the SiN^- anion using a highly accurate ab initio approach.

Experimentally, Meloni et al. [10] used anion photoelectron spectroscopy to obtain the $\text{SiN} (X^2\Sigma^+, A^2\Pi) + e^- \leftarrow \text{SiN}^- (X^1\Sigma^+)$ transitions for the first time in 2004. They determined the equilibrium bond length (R_e), harmonic frequency (ω_e), and dissociation energy (D_0) for the $X^1\Sigma^+$ state of SiN^- . The adiabatic electron affinity (AEA) of SiN was also determined.

Theoretically, only six groups of computations [11–16] were performed. In 1989, Peterson and Woods [11] used the Møller–Plesset perturbation theory with single, double, and quadruple

substitutions (MP4SDQ) and two large Gaussian basis sets to calculate the AEA ($26,826.21 \text{ cm}^{-1}$) of SiN and the spectroscopic constants of the SiN⁻ ($X^1\Sigma^+$). In 1992, McLean et al. [12] studied the potential energy curve (PEC) of SiN⁻ ($X^1\Sigma^+$) at the singles and double excitation from a single reference configuration interaction plus Davidson correction (SDCI + Q) levels of theory. Kalcher [13] in 2002 studied the AEA ($23,083.58 \text{ cm}^{-1}$) of SiN and the PECs of $X^1\Sigma^+$ and $a^3\Sigma^+$ states using the complete active space in conjunction with the averaged coupled pair functional (CAS-ACPF) approach using the cc-pVQZ basis set. In 2003, Midda and Das [14] calculated the spectroscopic constants and molecular properties of $X^1\Sigma^+$ states using a hybrid HF/DF B3LYP method with four different basis sets. Kerkinis and Mavridis [15] in 2005 calculated the spectroscopic constants and energetics for the SiN ($X^2\Sigma^+$, $A^2\Pi$) and SiN⁻ ($X^1\Sigma^+$, $a^3\Sigma^+$) at the level of the theory of the restricted coupled-cluster method with all singles and doubles and noniterative inclusion of triples [RCCSD(T)]. Their best estimated AEA is $24,212.75 \text{ cm}^{-1}$. Recently, Mogren et al. [16] used Gaussian-3 theory to study the R_e and ω_e of the $X^1\Sigma^+$ state of SiN⁻. Furthermore, they derived the AEA ($25,648.42 \text{ cm}^{-1}$) and vertical electron affinity (VEA = $24,115.97 \text{ cm}^{-1}$) at the MP2/6-31G* level. After summarizing these theoretical spectroscopic results [11–16], we firstly found that all of the calculations were mainly focused on the $X^1\Sigma^+$ and $a^3\Sigma^+$ states, and few results achieved high quality. Secondly, it was observed that no spin-orbit coupling (SOC) interactions were involved, though the SOC effect could influence the accurate prediction of spectroscopic properties [17,18]. Finally, it was found that no transition probabilities, such as Franck-Condon (FC) factors and the radiative lifetimes of the $a^3\Sigma^+_1$ ($v' = 0-2$) to $X^1\Sigma^+_{0+}$ transition, were calculated despite the fact that the transition probabilities were very useful in observing the corresponding states. Therefore, to improve the quality of the spectroscopic parameters of the anion, more accurate calculations should be done.

This paper is organized as follows. The methodology is briefly introduced in the next section. The PECs are reported in Section 3. The spectroscopic parameters and vibrational properties are predicted. The SOC effect on the spectroscopic parameters and vibrational levels is evaluated. The transition dipole moments (TDMs) between the $a^3\Sigma^+_1$ and $X^1\Sigma^+_{0+}$ states are determined. Calculations of FC factors and the radiative lifetimes of the $a^3\Sigma^+_1$ to $X^1\Sigma^+_{0+}$ transition are shown. Some conclusions are drawn in Section 4. The spectroscopic parameters, vibrational levels, and transition probabilities obtained here can be considered very reliable.

2. Methodology

The electron affinities of ground-state Si and N atoms are $11,207.24$ and -560 cm^{-1} [19], respectively. Thus, the first dissociation channel of the SiN⁻ anion should be Si⁻ (4S_u) + N (4S_u). The first and second excited states of Si⁻ anion are 2D_u and 2P_u ; their energy levels relative to the ground state (4S_u) are approximately 6961.85 and $(10,977.24 + x^e)/2 \text{ cm}^{-1}$ [19], respectively. The first excited state of the N atom is 2D_u ; its energy level relative to its ground state (4S_u) is approximately $19,228.82 \text{ cm}^{-1}$ [20]. Using the electron affinities and energy levels, we can determine that the second and third dissociation channels of the SiN⁻ anion are Si⁻ (2D_u) + N (4S_u) and Si⁻ (2P_u) + N (4S_u), respectively. With the help of group theory, 4 states ($X^1\Sigma^+$, $a^3\Sigma^+$, $1^5\Sigma^+$, and $1^7\Sigma^+$) were correlated to the first dissociation channel, 6 states ($b^3\Delta$, $c^3\Pi$, $d^3\Sigma^+$, $2^5\Sigma^+$, $1^5\Pi$, and $1^5\Delta$) were correlated to the second dissociation limit, and 4 states ($e^3\Sigma^-$, $1^5\Sigma^-$, $f^3\Pi$, and $2^5\Pi$) were correlated to the third dissociation limit. These states and asymptotes are collected in Table 1. Using the approaches outlined above, we have determined the energy separation between each higher dissociation channel and the lowest one, i.e., Si⁻ (4S_u) + N (4S_u). For reasons of comparison, we also collected the energy separation obtained using the icMRCI + Q/56 + CV + DK calculations and experiments [19] in Table 1. As seen in Table 1, the present results agree favorably with the measurements [19]. The results indicate that our calculations can properly describe the dissociation properties of SiN⁻.

Table 1. Dissociation relationships of the 14 states generated from the first three dissociation channels of the SiN[−] anion.

Dissociation Channel	Electronic State	Relative Energy/cm ^{−1}	
		This Work ^a	Exp. [19]
Si [−] (⁴ S _u) + N(⁴ S _u)	X ¹ Σ ⁺ , a ³ Σ ⁺ , 1 ⁵ Σ ⁺ , 1 ⁷ Σ ⁺	0.0	0.0
Si [−] (² D _u) + N(⁴ S _u)	b ³ Δ, c ³ Π, d ³ Σ ⁺ , 2 ⁵ Σ ⁺ , 1 ⁵ Π, 1 ⁵ Δ	6973.48	6961.85 ^b
Si [−] (² P _u) + N(⁴ S _u)	e ³ Σ [−] , 1 ⁵ Σ [−] , f ³ Π, 2 ⁵ Π	10,974.90	(10,977.24 + x ^c)/2

^a Obtained using the icMRCI + Q/56 + CV + DK calculations; ^b obtained by averaging the atomic energy levels of the ²D_{3/2} and ²D_{5/2} states; ^c no experimental energy level of ²P_{3/2} state obtained by Andersen et al. [19].

The PECs were calculated using the complete active space self-consistent field (CASSCF) method followed by the internally contracted multireference configuration interaction (icMRCI) plus the Davidson modification (icMRCI + Q) approach [21,22] for internuclear separations from approximately 0.10 to 1.08 nm. As a result, the CASSCF was used as the reference wavefunction for the icMRCI calculations. In the calculations for the Si and N atoms, the basis sets aug-cc-pV5Z (AV5Z) and aug-cc-pV6Z (AV6Z) [23,24] were employed. The calculations were done with the MOLPRO 2010.1 program package [25] in the C_{2v} point group. The point spacing interval used for calculating the PECs is 0.02 nm for each state. To accurately determine each PEC, the point spacing interval used was further reduced to 0.002 nm for internuclear separations from approximately 0.11 to 0.50 nm; this is because the equilibrium separations fall into this range for all the bound and quasi-bound states involved. It should be noted that these point spacing intervals were suitable for all the calculations including the core–valence correlation, scalar relativistic corrections, and the SOC effect.

The molecular orbitals (MOs) used for the icMRCI calculations come from the CASSCF results. The state-averaged technique was used in the CASSCF calculations. To accurately determine the interaction between different PECs (such as avoided crossings), we put the 18 electronic states together into the calculations. Each state has the same weight factor of 0.0588235. In this paper, we only reported the PECs of 14 states arising from the first three dissociation limits. In the icMRCI calculations, we put the 8 outermost MOs (4a₁, 2b₁, and 2b₂) into the active space. This corresponds to the 5-8σ, 2π, and 3π MOs in the anion. No additional MOs were included in the active space. That is, the 10 valence electrons were distributed into the 8 valence MOs of the SiN[−] anion. Consequently, this active space was referred to as CAS (10, 8). The rest of the 12 inner electrons were put into the 6 lowest MOs (4a₁, 1b₁, and 1b₂). For the AV6Z basis set, the total number of external orbitals is 368, corresponding to 126a₁, 90b₁, 90b₂, and 62a₂. In summary, we used 14 MOs (8a₁, 3b₁, and 3b₂) to calculate the PECs of all the 14 Λ-S states.

Scalar relativistic correction was computed using the cc-pV5Z-DK basis set [26]. Its contribution to the total energy is denoted as DK. The core-valence correlation correction was calculated with the cc-pCVTZ basis set [27]. Its contribution to the total energy is denoted as CV. The SOC effect was determined by the state interaction method with the Breit-Pauli operator [28] at the level of the icMRCI theory with the all-electron cc-pCVTZ basis set. The all-electron cc-pCVTZ basis set with and without the Breit-Pauli operator was used to calculate the contribution to potential energy via the SOC effect. The difference between the two energies is the SOC splitting energy, which is denoted as SOC. The extrapolation of potential energy to the complete basis set (CBS) limit was performed with the AV5Z and AV6Z basis sets. The energy obtained from the extrapolation is denoted as 56. The extrapolation scheme [29] is as follows:

$$\Delta E_X^{ref} = E_\infty^{ref} + A^{ref} X^{-\alpha} \quad (1)$$

$$\Delta E_X^{corr} = E_\infty^{corr} + A^{corr} X^{-\beta}. \quad (2)$$

Here, ΔE_X^{ref} and ΔE_X^{corr} are the CASSCF and correlation energies obtained by the aug-cc-pVXZ basis set, respectively. E_∞^{ref} and E_∞^{corr} are the CASSCF and correlation energies extrapolated to the CBS limit, respectively. The extrapolation parameters α and β are taken as 3.4 and 2.4 for the Hartree–Fock and correlation energies [29], respectively.

With the PECs, the spectroscopic parameters T_e , R_e , ω_e , $\omega_e x_e$, $\omega_e y_e$, α_e , B_e , and D_e were evaluated. The meanings of these spectroscopic notations are explained in our earlier paper [30,31]. All the PECs were fitted to an analytical form by cubic splines. The rovibrational constants were first obtained from the analytic potential by solving the rovibrational Schrödinger equation, and the spectroscopic parameters were then evaluated by fitting the vibrational levels.

3. Results and Discussion

Figures 1 and 2 show the PECs of 14 electronic states obtained by the icMRCI + Q/56 + CV + DK calculations. To clearly display the details of each PEC, we plotted them only over a small internuclear separation range from approximately 0.11 to 0.50 nm. The dissociation channel of each state is also indicated in the figure.

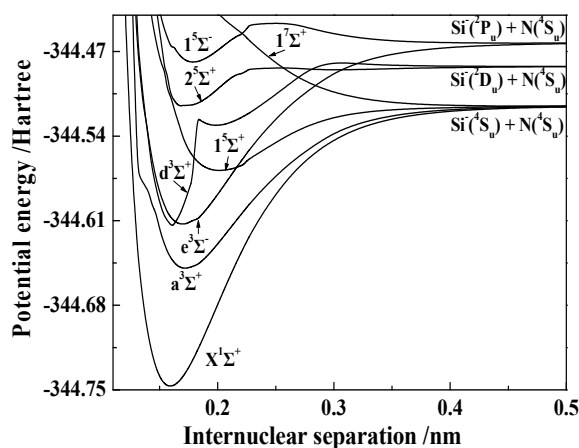


Figure 1. PECs of the 8 Λ -S states with the Σ symmetry of the SiN^- anion.

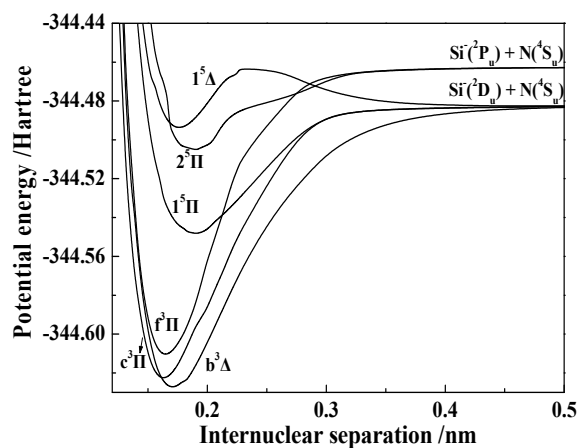


Figure 2. PECs of the 6 Λ -S states with the Π and Δ symmetries of the SiN^- anion.

From the PECs shown in Figures 1 and 2, we can summarize the following features. (1) All the bound states (i.e., $X^1\Sigma^+$, $a^3\Sigma^+$, $b^3\Delta$, $c^3\Pi$, $e^3\Sigma^-$, $f^3\Pi$, $1^5\Sigma^+$, $1^5\Pi$, and $2^5\Pi$) have a single well. (2) Two states, namely $1^5\Delta$ and $1^5\Sigma^-$, each have a single well and one barrier. The potential energies of the two barriers are obviously larger than those at their respective dissociation limits. (3) Besides the $1^5\Delta$ and $1^5\Sigma^-$ states,

the $d^3\Sigma^+$ and $2^5\Sigma^+$ states also have barriers on their PECs. In detail, the $d^3\Sigma^+$ state has a double well and two barriers; the $2^5\Sigma^+$ state has a double well and one barrier, but the second well of the $2^5\Sigma^+$ state is so shallow that it cannot be clearly distinguished. The barriers and the double wells of the $d^3\Sigma^+$ and $2^5\Sigma^+$ states will be discussed in detail later in this paper. (4) The $1^7\Sigma^+$ state is repulsive. (5) The avoided crossings are found in four paired states: the $2^3\Sigma^+$ and $3^3\Sigma^+$ states, the $2^5\Sigma^+$ and $3^5\Sigma^+$ states, the $1^5\Delta$ and $2^5\Delta$ states, and the $1^5\Sigma^-$ and $2^5\Sigma^-$ states.

To better study the transition probabilities between two electronic states, we present the leading valence electronic configurations of all the bound and quasi-bound states near their respective internuclear equilibrium positions in Table S1 of the Supporting Information section. These were determined by the icMRCI/AV6Z calculations. Due to length limitations, we only tabulated these valence configurations in Table S1 if the coefficients-squared of the configuration-state function (CSF) were larger than 0.1.

3.1. Electron Affinity of SiN and the Stable States of SiN⁻

3.1.1. Electron Affinity of SiN

At the icMRCI + Q/56 + CV + DK level of theory, the AEA and VEA of SiN are computed to be $23,262.27\text{cm}^{-1}$ and $22,766.75\text{cm}^{-1}$, respectively. These correspond to the SiN ($X^2\Sigma^+, v=0$) + $e^- \rightarrow$ SiN⁻ ($X^1\Sigma^+, v''=0$) and SiN ($X^2\Sigma^+, v=0$) + $e^- \rightarrow$ SiN⁻ ($X^1\Sigma^+, 0 < v'' < 1$) transitions, respectively. Our AEA agrees well with the experimental result of $23,785.28\text{cm}^{-1}$ [10]. Only the theoretical AEA obtained by Kerkinis and Mavridis [15] is slightly closer to the experimental result than this one. In addition, the vertical detachment energy (VDE) of SiN⁻ was calculated at the icMRCI + Q/56 + CV + DK level of theory as $23,639.13\text{cm}^{-1}$. This corresponds to the SiN ($X^2\Sigma^+, 0 < v^+ < 1$) + $e^- \leftarrow$ SiN⁻ ($X^1\Sigma^+, v''=0$) transition. The computed electron affinities adhere to the expected trend: VEA < AEA < VDE.

3.1.2. Spectroscopic Parameters of the 13 Stable and Metastable Λ -S States of SiN⁻

Employing the PECs determined by the icMRCI + Q/56 + CV + DK calculations, we evaluated the spectroscopic parameters of 13 Λ -S states. For the purposes of this discussion and due to length limitations, the spectroscopic parameters of the 13 Λ -S states are given in Table S2, along with the experimental only [10] and other theoretical [11–16] spectroscopic results.

The ground state $X^1\Sigma^+$ of the SiN⁻ anion is mainly characterized by the closed-shell electronic configuration $5\sigma^2 6\sigma^2 7\sigma^2 2\pi^4 3\pi^0 8\sigma^0$ (0.827). A group of experimental work [10] and six groups of calculations [11–16] reported the spectroscopic parameters of this state. Values of R_e and ω_e for this state obtained in this work deviate from the experimental values [10] by only 0.00117 nm and 8.87cm^{-1} , respectively. Using the values of ω_e , $\omega_e x_e$ and $\omega_e y_e$ obtained here in combination with the equation $D_e = D_0 + \omega_e/2 - \omega_e x_e/4 + \omega_e y_e/8$, we determined the ground state D_0 to be approximately 6.2466 eV. Obviously, the present D_0 is close to the experimental values [10] as the deviation is only 0.0066 eV. We found, as shown in Table 3, that only the theoretical R_e values obtained by Peterson and Woods [11] and Kalcher [13] are slightly closer to the measurements [10] than what we have obtained. This state has a well depth of approximately $50,592.79\text{cm}^{-1}$. It has 81 vibrational states, as tabulated in Table S3. Nevertheless, $X^1\Sigma^+ (v''=24)$ lies $23,613.44\text{cm}^{-1}$ above the $X^1\Sigma^+ (v''=0)$, which is larger than the calculated AEA. This means the $X^1\Sigma^+ v'' \geq 24$ vibrational levels are difficult to observe in a spectroscopy experiment.

The $a^3\Sigma^+$, $b^3\Delta$, $c^3\Pi$, $e^3\Sigma^-$, $f^3\Pi$, $1^5\Sigma^+$, $1^5\Pi$, and $2^5\Pi$ states also possess the single reference character near the equilibrium position. The dominant electronic configurations of the $a^3\Sigma^+$, $b^3\Delta$, $e^3\Sigma^-$, and $1^5\Sigma^+$ states arise from the $2\pi \rightarrow 3\pi$ singlet electronic excitation of the ground state. The dominant electronic configurations of the $c^3\Pi$ and $f^3\Pi$ states are generated predominantly from the $7\sigma \rightarrow 3\pi$ and $2\pi \rightarrow 8\sigma$ singlet electronic excitations of the ground state, respectively, whereas the dominant electronic configurations of the $1^5\Pi$ and $2^5\Pi$ states come from the $2\pi \rightarrow 3\pi$, $7\sigma \rightarrow 3\pi$, and $2\pi \rightarrow 3\pi$, $2\pi \rightarrow 8\sigma$ double electronic excitations of the ground state, respectively.

Two groups of calculations have been performed [13,15], but no measurements on the spectroscopic parameters of the $a^3\Sigma^+$ state had been reported. Compared with the results obtained by Kalcher [13], the present R_e and D_e results are slightly smaller, but the present ω_e and T_e values are obviously larger. In addition, the present T_e value is obviously smaller, but the present R_e and D_e values are larger than the previous results [15]. It should be noted that the previous results [13,15] were calculated using a small basis set [13] and the single reference method [15], whereas the present ones are derived by the icMRCI + Q method with extrapolation to the CBS limit and including various corrections. For this reason, we believe the present results should be more accurate and reliable [13,15]. To date, no experimental or other theoretical spectroscopic parameters have been reported in the literature for the $b^3\Delta$, $c^3\Pi$, $e^3\Sigma^-$, $f^3\Pi$, $1^5\Sigma^+$, $1^5\Pi$, or $2^5\Pi$ states.

For the $a^3\Sigma^+$ state, the depth of the well is approximately $29,492.12\text{ cm}^{-1}$. It has 68 vibrational states, as tabulated in Table S3. However, the $a^3\Sigma^+$ ($v' = 3$) lies $23,604.85\text{ cm}^{-1}$ above the $X^1\Sigma^+$ ($v'' = 0$), and is also larger than the calculated AEA. Hence, the $a^3\Sigma^+$ ($v' \geq 3$) would be metastable towards autodetachment.

As with $X^1\Sigma^+$ ($v'' \geq 24$) and $a^3\Sigma^+$ ($v' \geq 3$), the $b^3\Delta$, $c^3\Pi$, $e^3\Sigma^-$, $f^3\Pi$, $1^5\Sigma^+$, $1^5\Pi$, and $2^5\Pi$ states are metastable states.

Two-pair avoided crossings are located at approximately $R = 0.2284\text{ nm}$ (between the $1^5\Delta$ and $2^5\Delta$ states) as well as at approximately $R = 0.2604\text{ nm}$ (between the $1^5\Sigma^-$ and $2^5\Sigma^-$ states). Therefore, the $1^5\Delta$ and $1^5\Sigma^-$ states have a potential well induced by the avoided crossings in the range of $R < 0.2284$ and $R < 0.2604\text{ nm}$, respectively. They are repulsive at larger internuclear distances. The potential energy at the top of the barrier of each state is higher than that at their respective dissociation limits by approximately 4250.02 and 3750.36 cm^{-1} , respectively. Thus, both the dissociation energy and well depth of each state are relative to their respective barriers and are equal to 6696.83 and 7213.21 cm^{-1} , respectively. The $1^5\Delta$ and $1^5\Sigma^-$ states possess 11 and 12 vibrational states, respectively. These vibrational levels are summarized in Table S4. The dominant electronic transitions between the $1^5\Delta$ and $1^5\Pi$ states and between the $1^5\Sigma^-$ and $1^5\Pi$ states can be regarded as 3π to 8σ promotions.

The $d^3\Sigma^+$ state has a double well and two barriers. The two barriers lie at approximately 0.1824 and 0.3004 nm , respectively. They are formed by the avoided crossings of the $d^3\Sigma^+$ and $3^3\Sigma^+$ states. The potential energy at the top of the first barrier is lower, whereas that of the second barrier is higher than that at the dissociation limit for the $d^3\Sigma^+$ state. Therefore, the depths of the two wells should be relative to the first barrier, but their dissociation energies must be relative to the second barrier. The depth of the first well is approximately $19,808.90\text{ cm}^{-1}$. It has 12 vibrational states, as listed in Table S4. The depth of the second well is approximately 1355.04 cm^{-1} . It has three vibrational states, as presented in Table S4.

The $2^5\Sigma^+$ state has a double well and one barrier. The barrier is generated by the avoided crossing of this state with the $3^5\Sigma^+$ state at approximately 0.2604 nm . For the $2^5\Sigma^+$ state, the potential energy at the top of the barrier is lower than that at the dissociation limit. Thus, the depths of the double well should be relative to the barrier, whereas the dissociation energies of the double well must be relative to the dissociation limit. For the double well of the $2^5\Sigma^+$ state, the well depths are 6970.08 and 450.14 cm^{-1} , with 11 and 5 vibrational levels, respectively. These vibrational levels are presented in Table S4.

As with the $b^3\Delta$, $c^3\Pi$, $e^3\Sigma^-$, $f^3\Pi$, $1^5\Sigma^+$, $1^5\Pi$, and $2^5\Pi$ states, neither theoretical nor experimental studies have been reported in the literature regarding the $1^5\Delta$, $1^5\Sigma^-$, $d^3\Sigma^+$, and $2^5\Sigma^+$ metastable states.

3.2. Spectroscopic Parameters and Vibrational Levels of the 45 Ω Bound States

When the SOC is taken into account, the $\text{Si}^-(^4S_u) + \text{N}(^4S_u)$ dissociation channel splits into one dissociation asymptote. Each of the $\text{Si}^-(^2D_u) + \text{N}(^4S_u)$ and $\text{Si}^-(^2P_u) + \text{N}(^4S_u)$ dissociation limits splits into two asymptotes. These Ω states and their dissociation asymptotes are listed in Table 2. In employing the icMRCI + Q/56 + CV + DK + SOC calculations, we determined the energy separations between each higher asymptote and the lowest one, i.e., $\text{Si}^-(^4S_u) + \text{N}(^4S_u)$. The dissociation relationships for the possible Ω states and corresponding energy separations are

also listed in Table 2. Simultaneously, we also collected the corresponding experimental energy separations [19] for comparison. As seen in Table 2, the energy separations obtained in this paper agree favorably with the experimental values [19].

The 14 Λ -S states are split into 49 Ω states. In detail, 10 Ω states ($X^1\Sigma^+_{0+}$, $a^3\Sigma^+_{1-}$, $a^3\Sigma^+_{0-}$, $1^5\Sigma^+_{2-}$, $1^5\Sigma^+_{1-}$, $1^5\Sigma^+_{0+}$, $1^7\Sigma^+_{0-}$, $1^7\Sigma^+_{1-}$, $1^7\Sigma^+_{2-}$, and $1^7\Sigma^+_{3-}$) arise from the $\text{Si}^-(^4\text{S}_{3/2}) + \text{N}(^4\text{S}_{3/2})$ channel, 10 Ω states ($c^3\Pi_{0-}$, $c^3\Pi_{0+}$, $c^3\Pi_1$, $c^3\Pi_2$, $1^5\Pi_3$, $1^5\Pi_2$, $1^5\Pi_1$, $1^5\Pi_{0+}$, $1^5\Pi_{0-}$, and $1^5\Pi_{-1}$) are produced from the $\text{Si}^-(^2\text{D}_{3/2}) + \text{N}(^4\text{S}_{3/2})$ channel, 14 Ω states ($b^3\Delta_1$, $b^3\Delta_2$, $b^3\Delta_3$, $d^3\Sigma^+_{0-}$, $d^3\Sigma^+_{1-}$, $1^5\Delta_{0-}$, $1^5\Delta_{0+}$, $1^5\Delta_1$, $1^5\Delta_2$, $1^5\Delta_3$, $1^5\Delta_4$, $2^5\Sigma^+_{2-}$, $2^5\Sigma^+_{1-}$, and $2^5\Sigma^+_{0+}$) are associated with the $\text{Si}^-(^2\text{D}_{5/2}) + \text{N}(^4\text{S}_{3/2})$ asymptote, 5 Ω states ($2^5\Pi_{-1}$, $2^5\Pi_{0-}$, $2^5\Pi_{0+}$, $2^5\Pi_1$, and $2^5\Pi_2$) are yielded from the $\text{Si}^-(^2\text{P}_{1/2}) + \text{N}(^4\text{S}_{3/2})$ asymptote, and 10 Ω states ($e^3\Sigma^-_{0+}$, $e^3\Sigma^-_{-1}$, $f^3\Pi_2$, $f^2\Pi_1$, $f^3\Pi_{0+}$, $f^3\Pi_{0-}$, $2^5\Pi_3$, $1^5\Sigma^-_{0-}$, $1^5\Sigma^-_{-1}$, and $1^5\Sigma^-_{-2}$) belong to the $\text{Si}^-(^2\text{P}_{3/2}) + \text{N}(^4\text{S}_{3/2})$ channel. Of these 49 Ω states, only the $1^7\Sigma^+_{0-}$, $1^7\Sigma^+_{1-}$, $1^7\Sigma^+_{2-}$, and $1^7\Sigma^+_{3-}$ states are repulsive.

Table 2. Dissociation relationships of possible Ω states yielded from the first three dissociation channels of the SiN^- anion.

Atomic State	Possible Ω States	Relative Energy/cm ⁻¹	
		This Work ^a	Exp. [19]
$\text{Si}^-(^4\text{S}_{3/2}) + \text{N}(^4\text{S}_{3/2})$	$0^-(2), 0^+(2), 1(3), 2(2), 3$	0.00	0.00
$\text{Si}^-(^2\text{D}_{3/2}) + \text{N}(^4\text{S}_{3/2})$	$-1, 0^-(2), 0^+(2), 1(2), 2(2), 3$	6968.32	6954.81
$\text{Si}^-(^2\text{D}_{5/2}) + \text{N}(^4\text{S}_{3/2})$	$0^-(2), 0^+(2), 1(4), 2(3), 3(2), 4$	6978.63	6968.89
$\text{Si}^-(^2\text{P}_{1/2}) + \text{N}(^4\text{S}_{3/2})$	$-1, 0^-, 0^+, 1, 2$	10,970.08	10,977.24
$\text{Si}^-(^2\text{P}_{3/2}) + \text{N}(^4\text{S}_{3/2})$	$0^-(2), 0^+(2), 1(3), 2(2), 3$	10,979.76	x^b

^a Obtained by the icMRCI + Q/56 + CV + DK + SOC calculations; ^b no experimental energy level of $^2\text{P}_{3/2}$ state obtained by Andersen et al. [19].

To conveniently discuss the spectroscopic parameters and vibrational levels of these Ω states, we divide them into three types according to their symmetries. The first group comprises 16 Ω states, which arise from the $X^1\Sigma^+$, $a^3\Sigma^+$, $d^3\Sigma^+$, $e^3\Sigma^-$, $1^5\Sigma^+$, $2^5\Sigma^+$, and $1^5\Sigma^-$ states. The second group comprises 20 Ω states, which come from the $c^3\Pi$, $f^3\Pi$, $1^5\Pi$, and $2^5\Pi$ states. The third group comprises nine Ω states, which are generated from the $b^3\Delta$ and $1^5\Delta$ states.

3.2.1. Spectroscopic and Vibrational Properties of 16 Ω States with the Σ Symmetry

Using the PECs obtained by the icMRCI + Q/56 + CV + DK + SOC calculations, we evaluated the T_e , D_e , R_e , and ω_e values of these 16 Ω states with Σ symmetry. The spectroscopic parameters are presented in Table S5. For reasons of discussion, the leading Λ -S state compositions of each Ω state near their respective equilibrium positions are also presented in Table S5. For clarity, we neglected the Λ -S states that contribute less than 0.08% to the total Λ -S state composition.

The $X^1\Sigma^+$ state does not split when the SOC effect is included. The $X^1\Sigma^+_{0+}$ state completely consists of the $X^1\Sigma^+$ state in the FC region. Comparing R_e , ω_e , and D_e values collected in Tables S2 and S5, we confirmed that the SOC effect on these spectroscopic parameters can be negligible. Additionally, the vibrational levels of $X^1\Sigma^+_{0+}$ states are almost equal to the corresponding values of the $X^1\Sigma^+$ state.

The SOC interaction causes the $a^3\Sigma^+$ and $e^3\Sigma^-$ states to split into four Ω states: $a^3\Sigma^+_{1-}$, $a^3\Sigma^+_{0-}$, $e^3\Sigma^-_{0+}$, and $e^3\Sigma^-_{-1}$, in the order of increasing energy. The $a^3\Sigma^+$ state is inverted, whereas the $e^3\Sigma^-_{-1}$ state is regular when the SOC effect is taken into account. The SOC effect on the R_e , ω_e , and D_e values of these two states is small. This is consistent with the fact that the Λ -S state compositions of each Ω state are almost pure near their respective equilibrium positions. The SOC splitting energies of $a^3\Sigma^+$ and $e^3\Sigma^-$ states are only 0.87 and 0.88 cm⁻¹, respectively. This is not large. In comparing the T_e , R_e , ω_e , and D_e values of each Ω state with those seen in Table S2, we affirm that the difference between them is small. This shows that the SOC effect is very small in the spectroscopic parameters of these Ω states. In addition, the SOC effect on their vibrational levels is also small.

Under the SOC effect, the $d^3\Sigma^+$ state is regular and still has a double well. As seen in Table S5, for the double well, the Λ -S state compositions of each Ω state are pure around their respective equilibrium positions. Accordingly, the spectroscopic parameters and vibrational levels of the $d^3\Sigma^+_{0-}$ and $d^3\Sigma^+_{1}$ states are almost equal to those of the $d^3\Sigma^+$ state for both the first and second well.

Each of the $1^5\Sigma^+$ and $1^5\Sigma^-$ states splits into three Ω states with the SOC effect taken into account. As seen in Table S5, the Λ -S state compositions of each Ω state are almost pure around their respective equilibrium positions. Accordingly, the SOC effect on their spectroscopic parameters is small. Through comparison, we confirm that the SOC effect on their vibrational levels is also very small. In addition, the $1^5\Sigma^+$ state is inverted when the SOC effect is included.

The $2^5\Sigma^+_{2}$, $2^5\Sigma^+_{1}$, and $2^5\Sigma^+_{0+}$ states have a double well. The T_e of the $2^5\Sigma^+_{2}$ state is smaller than that of the $2^5\Sigma^+_{0+}$ state for both the first and second well. Therefore, the $2^5\Sigma^+$ state is inverted when the SOC effect is taken into account. For the first well, as seen in Table S5, the Λ -S state compositions of each Ω state are pure near the equilibrium positions. This is also true with the $1^5\Sigma^+$ and $1^5\Sigma^-$ states. The SOC effect on the spectroscopic parameters and vibrational levels of all the Ω states is tiny. For the second well, the Λ -S state compositions of the three Ω states slightly mix with the $c^3\Pi$ and $1^5\Pi$ states near their respective equilibrium positions. The largest deviations of R_e , ω_e , and D_e values of each Ω state from those originating from the $2^5\Sigma^+$ state are 0.00019 nm, 1.275 cm^{-1} , and 0.0003 eV, respectively. The SOC splitting energies between the two neighboring Ω states from $2^5\Sigma^+_{2}$ to $2^5\Sigma^+_{0+}$ are only 0.65 and 0.22 cm^{-1} , respectively. Each Ω state has five vibrational levels, which are almost equal to those of the second well of the $2^5\Sigma^+$ state.

In conclusion, (1) the $a^3\Sigma^+$, $1^5\Sigma^+$ and $2^5\Sigma^+$ states are inverted with the SOC effect taken into account. (2) The SOC effect to the spectroscopic parameters and the vibrational levels of all the Σ states is small.

3.2.2. Spectroscopic and Vibrational Properties of 20 Ω States with the Π Symmetry

Using the PECs obtained by the icMRCI + Q/56 + CV + DK + SOC calculations, we evaluated T_e , R_e , ω_e , and D_e values of the 20 Ω states with the Π symmetry. The spectroscopic parameters are tabulated in Table S6. As with Table S5, also presented the leading Λ -S state compositions of each Ω state around their respective equilibrium positions.

The $c^3\Pi$ state splits into four Ω states (i.e., $c^3\Pi_{0-}$, $c^3\Pi_{0+}$, $c^3\Pi_1$, and $c^3\Pi_2$) when the SOC effect is accounted for. The SOC splitting energies between two consecutive Ω states from the $c^3\Pi_{0-}$ to $c^3\Pi_2$ states are 0.44, 47.19, and 47.62 cm^{-1} , respectively. These are relatively large when compared with those of other states. The SOC effect on R_e , ω_e and D_e values of each Ω state is not large. The largest deviations of R_e , ω_e , and D_e values of all four Ω states of the split $c^3\Pi$ state are 0.00002 nm, 0.274 cm^{-1} , and 0.0059 eV, respectively. In comparison, we can confirm that the SOC effect on the vibrational levels of these Ω states is also small.

Under the SOC effect, the $f^3\Pi$ also splits into four Ω states ($f^3\Pi_{0-}$, $f^3\Pi_{0+}$, $f^3\Pi_1$, and $f^3\Pi_2$). Their energies increase in the order of $f^3\Pi_{0-}$, $f^3\Pi_{0+}$, $f^3\Pi_1$, and $f^3\Pi_2$ in the range of $R < 0.1644\text{ nm}$. However, the order of $f^3\Pi_{0-}$, $f^3\Pi_{0+}$, $f^3\Pi_1$, and $f^3\Pi_2$ changes in the internuclear distance region from 0.1644 to 1.08 nm. This phenomenon leads to the obvious change of the PECs for the $f^3\Pi_{0-}$, $f^3\Pi_{0+}$, and $f^3\Pi_2$ states. As a result, the spectroscopic parameters and the vibrational levels of $f^3\Pi_{0-}$, $f^3\Pi_{0+}$, and $f^3\Pi_2$ states are obviously different from those of the corresponding Λ -S state.

Each of the $1^5\Pi$ and $2^5\Pi$ states splits into six Ω states with the SOC effect taken into account, and the $1^5\Pi$ state is inverted. For the $1^5\Pi$ state, the largest deviations of R_e , ω_e , and D_e of each Ω state from those of the $1^5\Pi$ state are 0.00001 nm, 0.298 cm^{-1} , and 0.0047 eV, respectively; the SOC splitting energies between the two neighboring Ω states from the $1^5\Pi_3$ to the $1^5\Pi_{-1}$ are only 17.99, 18.22, 18.31, 0.13, and 18.65 cm^{-1} , respectively; on the whole, the SOC effect on the splitting energies is not large; each Ω state has 38 vibrational levels, which are almost equal to those of the first well of $1^5\Pi$ state. For the $2^5\Pi$ state, the Λ -S state compositions of each Ω state are pure near the equilibrium positions; as with the $c^3\Pi$ and $1^5\Pi$ states, the SOC effect on R_e , ω_e and D_e of all the Ω states is tiny; each Ω state

has the 36 vibrational states, in which vibrational levels are almost equal to those of the $2^5\Pi$ state; the energy splitting of $2^5\Pi_{-1}$ to $2^5\Pi_{0-}$, $2^5\Pi_{0-}$ to $2^5\Pi_{0+}$, $2^5\Pi_{0+}$ to $2^5\Pi_1$, $2^5\Pi_1$ to $2^5\Pi_2$, and $2^5\Pi_2$ to $2^5\Pi_3$ are 22.17, 0.22, 21.95, 22.16, and 22.17 cm^{-1} , respectively, which are not large; thus, we affirm that the SOC effect on the spectroscopic and vibrational properties of all the 6 Ω states is very small.

Our conclusions are as follows: (1) the SOC effect on the spectroscopic parameters is tiny except for the $f^3\Pi$ state and the spitting energies of $c^3\Pi$ state; (2) the $1^5\Pi$ state is inverted, and the $f^3\Pi$ state is also inverted in the internuclear distance range from 0.1644 to 1.08 nm with the SOC effect taken into account; (3) the SOC effect on the vibrational levels of all the Π states is small expect for the $f^3\Pi_{0-}$, $f^3\Pi_{0+}$, and $f^3\Pi_2$ states.

3.2.3. Spectroscopic and Vibrational Properties of Nine Ω States with the Δ Symmetry

Using the PECs obtained by the icMRCI + Q/56 + CV + DK + SOC calculations, we evaluated the T_e , D_e , R_e , and ω_e values of nine Ω states with the Δ symmetry. The spectroscopic parameters are presented in Table S7. As with Tables S5 and S6, the leading Λ -S state compositions of each Ω state around their respective internuclear equilibrium positions are also tabulated in Table S7.

The $b^3\Delta$ state splits into three Ω states when the SOC effect is taken into account. For the three Ω states, the energy arrangement from low to high is $b^3\Delta_3$, $b^3\Delta_2$, and $b^3\Delta_1$. The T_e , R_e , ω_e , and D_e values of each Ω state are very close to those of the $b^3\Delta$ state. Each Ω state has 70 vibrational states, the vibrational levels of which are almost equal to those of the $b^3\Delta$ state. As a result, we conclude that the SOC effect on the spectroscopic parameters and vibrational states is tiny.

The $1^5\Delta$ state splits into the $1^5\Delta_{0-}$, $1^5\Delta_{0+}$, $1^5\Delta_1$, $1^5\Delta_2$, $1^5\Delta_3$, and $1^5\Delta_4$ states when the SOC effect is included, as tabulated in Table S7. The Λ -S state compositions of each Ω state are almost pure around the internuclear equilibrium positions. Consequently, the SOC effect on the spectroscopic parameters and vibrational levels of each Ω state are inconspicuous.

In conclusion, (1) the SOC effect on the spectroscopic parameters and vibrational properties of the $b^3\Delta$ and $1^5\Delta$ states is very small, and (2) the $b^3\Delta$ state is inverted.

3.3. Transition Properties

The TDMs between the $a^3\Sigma^+_1$ and $X^1\Sigma^+_{0+}$ states were obtained with the Breit-Pauli Hamiltonian in combination with the all-electron CVTZ basis set at the level of the icMRCI theory. The curves of TDM versus internuclear separation are depicted in Figure 3. As with the PECs, to clearly show the main features of each TDM curve, we display them over a small range of internuclear separations. The figure clearly shows that the TDMs of the transitions from the $a^3\Sigma^+_1$ state to the $X^1\Sigma^+_{0+}$ state very small in the FC region. This is consistent with the fact that the triplet-singlet transitions are forbidden. In addition, the TDMs go to the zero asymptote when the internuclear distance is larger than 0.4 nm.

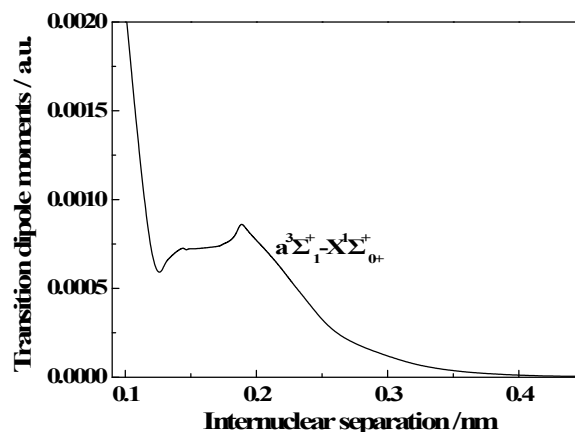


Figure 3. TDMs versus internuclear separations of transitions from the $a^3\Sigma^+_1$ state to the $X^1\Sigma^+_{0+}$ state.

Using the PECs and TDMs obtained here, we calculated the FC factors and Einstein coefficients of the $a^3\Sigma^+_1$ ($v' = 0-2$) to $X^1\Sigma^+_{0+}$ with the LEVEL program [32]. We only list the lowest 10 vibrational levels of the $X^1\Sigma^+_{0+}$ state due to the length limitation. For the purposes of this discussion, we present these results in Table 3. Table 4 lists the radiative lifetimes for the $a^3\Sigma^+_1$ ($v' = 0-2$) to $X^1\Sigma^+_{0+}$ transition. Overall, the $a^3\Sigma^+_1$ states are not easy to detect spectroscopically by observing these transitions. This can be explained based on the data in Tables 3 and 4. As presented in Tables 3 and 4, almost all of the Einstein coefficients of the $a^3\Sigma^+_1$ to $X^1\Sigma^+_{0+}$ transition are very small and their radiative lifetimes are very long. That is, these transitions are weak.

Table 3. FC factors (1st line) and Einstein coefficients (s^{-1} , 2nd line) for the $a^3\Sigma^+_1$ to $X^1\Sigma^+_{0+}$ transition.

State to State	$v'' = 0$	$v'' = 1$	$v'' = 2$	$v'' = 3$	$v'' = 4$	$v'' = 5$	$v'' = 6$	$v'' = 7$	$v'' = 8$	$v'' = 9$
$a^3\Sigma^+_1$ to $X^1\Sigma^+_{0+}$										
$v' = 0$	0.0970	0.2393	0.2796	0.2068	0.1099	0.0457	0.0159	0.0047	0.0011	0.0002
	0.3370	0.7136	0.7129	0.4506	0.2054	0.0736	0.0220	0.0056	0.0012	0.0002
$v' = 1$	0.1886	0.1666	0.0131	0.0455	0.1663	0.1929	0.1328	0.0644	0.0230	0.0057
	0.7245	0.5493	0.0359	0.1140	0.3519	0.3484	0.2064	0.0870	0.0274	0.0062
$v' = 2$	0.2373	0.0262	0.0709	0.1362	0.0207	0.0289	0.1378	0.1661	0.1101	0.0479
	1.0072	0.0954	0.2258	0.3692	0.0462	0.0613	0.2448	0.2544	0.1468	0.0556

Table 4. Radiative lifetime values of the transition from the $a^3\Sigma^+_1$ ($v' = 0-2$) excited Ω states to the $X^1\Sigma^+_{0+}$ state for the SiN^- anion.

Radiative Lifetimes			
Transitions	$v' = 0$	$v' = 1$	$v' = 2$
$a^3\Sigma^+_1$ to $X^1\Sigma^+_{0+}$ (ms)	396.5	407.9	396.4

4. Conclusions

In this work, we calculated the PECs of 14 Λ -S states of the SiN^- anion using the icMRCI + Q/56 + CV + DK approach, computed the TDMs of the $a^3\Sigma^+_1$ to $X^1\Sigma^+_{0+}$ transition using the icMRCI approach with the all-electron CVTZ basis set, and determined the spectroscopic parameters of 49 Ω states employing the icMRCI + Q/56 + CV + DK + SOC method. The spectroscopic parameters and vibrational levels were evaluated. In addition, the transition probabilities of $a^3\Sigma^+_1$ to $X^1\Sigma^+_{0+}$ were studied. These results were compared in detail with those reported in the literature. Excellent agreement is found between these results and those of other measurements. Of these 14 states, only the $1^7\Sigma^+$ state is repulsive. The avoided crossings exist between the $d^3\Sigma^+$ and $3^3\Sigma^+$ states, between the $2^5\Sigma^+$ and $3^5\Sigma^+$ states, between the $1^5\Delta$ and $2^5\Delta$ states, and between the $1^5\Sigma^-$ and $2^5\Sigma^-$ states. The $X^1\Sigma^+$ ($v'' \geq 24$), $a^3\Sigma^+$ ($v' \geq 3$), $b^3\Delta$, $c^3\Pi$, $d^3\Sigma^+$, $e^3\Sigma^-$, $f^3\Pi$, $1^5\Sigma^+$, $1^5\Pi$, $2^5\Sigma^+$, $2^5\Pi$, $1^5\Delta$, and $1^5\Sigma^-$ states are metastable states. The $d^3\Sigma^+$, $b^3\Delta$, $f^3\Pi$, $1^5\Sigma^+$, $1^5\Pi$, and $2^5\Sigma^-$ states are inverted when the SOC effect is included. The SOC effect on the spectroscopic parameters and vibrational levels is small except for in the $f^3\Pi$ state and the spitting energies of $c^3\Pi$ state. The spectroscopic parameters, vibrational levels, and transition probabilities obtained in this paper can be considered very reliable and can be employed as helpful guidelines for detecting these states in an appropriate spectroscopy experiment in the near future. In addition, the data provided in this work should assist in spectral searches for this anion in the interstellar medium.

Supplementary Materials: The supplementary materials are available online.

Acknowledgments: This work was sponsored by the National Natural Science Foundation of China under Grant No. 11274097 and the Program for Science and Technology of Henan Province in China under Grant No. 142300410201.

Author Contributions: Wei Xing computed the data and wrote the manuscript. Deheng Shi and Zunlue Zhu analyzed the data. Jinfeng Sun revised the manuscript and conceived and designed the project.

Conflicts of Interest: The authors declare no conflict of interest.

References

1. Agúndez, M.; Cernicharo, J.; Guélin, M.; Kahane, C.; Roueff, E.; Klos, J.; Aoiz, F.J.; Lique, F.; Marcelino, N.; Goicoechea, J.R.; et al. Astronomical identification of CN^- , the smallest observed molecular anion. *Astron. Astrophys.* **2010**, *517*, L2. [[CrossRef](#)]
2. Turner, B.E. Detection of SiN in IRC + 10216. *Astrophys. J.* **1992**, *388*, L35–L38. [[CrossRef](#)]
3. Guélin, M.; Muller, S.; Cernicharo, J.; Apponi, A.J.; McCarthy, M.C.; Gottlieb, C.A.; Thaddeus, P. Astronomical detection of the free radical SiCN. *Astrophys. J.* **2000**, *363*, L9–L12.
4. Guélin, M.; Muller, S.; Cernicharo, J.; McCarthy, M.C.; Thaddeus, P. Detection of the SiNC Radical in IRC + 10216. *Astron. Astrophys.* **2004**, *426*, L49–L52. [[CrossRef](#)]
5. Fortenberry, R.C.; Daniel Crawford, T. Theoretical prediction of new dipole-bound singlet states for anions of interstellar interest. *J. Chem. Phys.* **2011**, *134*, 154304. [[CrossRef](#)] [[PubMed](#)]
6. Drzaic, P.S.; Marks, J.; Brauman, J.I. *Gas-Phase Ion Chemistry*; Academic Press: New York, NY, USA, 1984; pp. 1–63.
7. Damrauer, R.; Hankin, J.A. Chemistry and thermochemistry of silicon-containing anions in the gas phase. *Chem. Rev.* **1995**, *95*, 1137–1160. [[CrossRef](#)]
8. Zhu, W.; Kochanski, G.P.; Jin, S. Low-field electron emission from undoped nanostructured diamond. *Science* **1998**, *282*, 1471–1473. [[CrossRef](#)] [[PubMed](#)]
9. Shabanov, S.V.; Gornushkin, I.B. Anions in laser-induced plasmas. *Appl. Phys. A* **2016**, *122*, 676. [[CrossRef](#)]
10. Meloni, G.; Sheehan, S.M.; Ferguson, M.J.; Neumark, D.M. Negative ion photoelectron spectroscopy of SiN^- . *J. Phys. Chem. A* **2004**, *108*, 9750–9754. [[CrossRef](#)]
11. Peterson, K.A.; Woods, R.C. Ground state spectroscopic and thermodynamic properties of AlO^- , SiN^- , CP^- , BS^- , BO^- , and CN^- from Møller-Plesset perturbation theory. *J. Chem. Phys.* **1989**, *90*, 7239–7250. [[CrossRef](#)]
12. McLean, A.D.; Liu, B.; Chandler, G.S. Computed self-consistent field and singles and doubles configuration interaction spectroscopic data and dissociation energies for the diatomics B_2 , C_2 , N_2 , O_2 , F_2 , CN , CP , CS , PN , SiC , SiN , SiO , SiP , and their ions. *J. Chem. Phys.* **1992**, *97*, 8459–8464. [[CrossRef](#)]
13. Kalcher, J. Trends in ground and excited state electron affinities of group 14, 15, and 16 mixed diatomic anions: A computational study. *Phys. Chem. Chem. Phys.* **2002**, *4*, 3311–3317. [[CrossRef](#)]
14. Midda, S.; Das, A.K. Theoretical study of spectroscopic constants and molecular properties of diatomic anions using B3LYP method. *J. Mol. Struct.* **2003**, *640*, 183–189. [[CrossRef](#)]
15. Kerkines, I.S.K.; Mavridis, A. On the electron affinity of SiN and spectroscopic constants of SiN^- . *J. Chem. Phys.* **2005**, *123*, 124301. [[CrossRef](#)] [[PubMed](#)]
16. Mogren, M.M.A.; El-Azhary, A.A.; Alkiali, W.Z.; Hochlaf, M. Electronic structure and properties of neutral, anionic and cationic silicon-nitrogen nanoclusters. *J. Mol. Model.* **2013**, *19*, 2657–2668. [[CrossRef](#)] [[PubMed](#)]
17. Luo, W.; Li, R.; Gai, Z.Q.; Ai, R.B.; Zhang, H.M.; Zhang, X.M.; Yan, B. Configuration interaction studies on the spectroscopic properties of PbO including spin-Orbit coupling. *Chin. Phys. B* **2016**, *25*, 073101. [[CrossRef](#)]
18. Zhao, S.T.; Yan, B.; Li, R.; Wu, S.; Wang, Q.L. MRCI + Q study of the low-lying electronic states of CdF including spin-orbit coupling. *Chin. Phys. B* **2017**, *26*, 023105. [[CrossRef](#)]
19. Andersen, T.; Haugen, H.K.; Hotop, H. Binding energies in atomic negative ions: III. *J. Phys. Chem. Ref. Data* **1999**, *28*, 1511–1533. [[CrossRef](#)]
20. Moore, C.E. *CRC Series in Evaluated Data in Atomic Physics*; CRC Press: Boca Raton, FL, USA, 1993; p. 339.
21. Langhoff, S.R.; Davidson, E.R. Configuration interaction calculations on the nitrogen molecule. *Int. J. Quantum. Chem.* **1974**, *8*, 61–72. [[CrossRef](#)]
22. Richartz, A.; Buenker, R.J.; Peyerimhoff, S.D. Ab initio MRD-CI study of ethane: The 14–25 eV PES region and Rydberg states of positive ions. *Chem. Phys.* **1978**, *28*, 305–312. [[CrossRef](#)]
23. Van Mourik, T.; Wilson, A.K.; Dunning, T.H. Benchmark calculations with correlated molecular wavefunctions. XIII. Potential energy curves for He_2 , Ne_2 and Ar_2 using correlation consistent basis sets through augmented sextuple zeta. *Mol. Phys.* **1999**, *99*, 529–547. [[CrossRef](#)]
24. Woon, D.E.; Dunning, T.H. Gaussian basis sets for use in correlated molecular calculations. III. The atoms aluminum through argon. *J. Chem. Phys.* **1993**, *98*, 1358–1371. [[CrossRef](#)]

25. Werner, H.-J.; Knowles, P.J.; Lindh, R.; Knizia, G.; Manby, F.R.; Schütz, M.; Celani, P.; Györfy, W.; Kats, D.; Korona, T.; et al. MOLPRO 2010.1 is a Package of Ab Initio Programs. Available online: <http://www.molpro.net> (accessed on 17 September 2010).
26. De Jong, W.A.; Harrison, R.J.; Dixon, D.A. Parallel Douglas-Kroll energy and gradients in NWChem: Estimating scalar relativistic effects using Douglas-Kroll contracted basis sets. *J. Chem. Phys.* **2001**, *114*, 48–53. [[CrossRef](#)]
27. Woon, D.E.; Dunning, T.H. Gaussian basis sets for use in correlated molecular calculations. V. Core-valence basis sets for boron through neon. *J. Chem. Phys.* **1995**, *103*, 4572–4585. [[CrossRef](#)]
28. Berning, A.; Schweizer, M.; Werner, H.-J.; Knowles, P.J.; Palmieri, P. Spin-orbit matrix elements for internally contracted multireference configuration interaction wavefunctions. *Mol. Phys.* **2000**, *98*, 1823–1833.
29. Oyeyemi, V.B.; Krisiloff, D.B.; Keith, J.A.; Libisch, F.; Pavone, M.; Carter, E.A. Size-extensivity-corrected multireference configuration interaction schemes to accurately predict bond dissociation energies of oxygenated hydrocarbons. *J. Chem. Phys.* **2014**, *140*, 044317. [[CrossRef](#)] [[PubMed](#)]
30. Xing, W.; Shi, D.H.; Sun, J.F.; Zhu, Z.L. Calculations of 21 Λ -S and 42 Ω states of BC molecule: Potential energy curves, spectroscopic parameters and spin-orbit coupling effect. *Spectrochim. Acta Part A Mol. Biomol. Spectrosc.* **2016**, *153*, 722–734. [[CrossRef](#)] [[PubMed](#)]
31. Xing, W.; Shi, D.H.; Sun, J.F.; Zhu, Z.L. Accurate spectroscopic calculations of the 19 Λ -S states and 36 Ω states of the BC⁺ cation. *Mol. Phys.* **2017**, *115*, 387–402. [[CrossRef](#)]
32. Le Roy, R.J. *LEVEL 8.0: A Computer Program for Solving the Radial Schrödinger Equation for Bound and Quasi-Bound Levels*; University of Waterloo Chemical Physics Research Report CP-663; University of Waterloo: Waterloo, ON, Canada, 2007.

Sample Availability: Not Available.



© 2018 by the authors. Licensee MDPI, Basel, Switzerland. This article is an open access article distributed under the terms and conditions of the Creative Commons Attribution (CC BY) license (<http://creativecommons.org/licenses/by/4.0/>).